STRONG SUPPRESSION OF ELECTRONIC COHERENCE TIME BY FLEXURAL PHONONS IN GRAPHENE — EXAMPLE OF A NEW DEPHASING MECHANISM

A Thesis

by

WEI ZHAO

Submitted to the Office of Graduate and Professional Studies of
Texas A&M University
in partial fulfillment of the requirements for the degree of

MASTER OF SCIENCE

Chair of Committee,	Alexander Finkel'stein
Committee Members,	Valery Pokrovsky
	Peter Kuchment
Head of Department,	George Welch

August 2014

Major Subject: Physics

ABSTRACT

We investigate decoherence of an electron in graphene caused by electron-flexural phonon interaction. We find out that the flexural phonons can produce dephasing rate comparable to the electron-electron one. The problem appears to be quite special because there is a large interval of temperatures where dephasing rate cannot be obtained using the golden rule. We evaluate this rate for a wide range of n and T and determine several asymptotic regions with temperature dependence crossing over from $\tau_\phi^{-1} \sim T^2$ to $\tau_\phi^{-1} \sim T$ when temperature increases. We also find τ_ϕ^{-1} to be a non-monotonous function of n. These distinctive features of the new contribution can provide an effective way to identify flexural phonons in graphene through the electronic transport by measuring the weak localization corrections in magnetoresistance.

DEDICATION

To my parents.

ACKNOWLEDGEMENTS

First of all, I would like to thank my advisor Dr. Sasha Finkel'stein for his continuous support and advice during my research work during my Master's study. Especially, I should admit that without his infinite patience and numerous guidance, it would be impossible for me to obtain any meaningful result in the project. I would also thank Sasha for bringing me the chances to spend nearly two years as a visiting student in the Weizmann Institute of Science (Israel) and Karlsruhe Institute of Technology (Germany). The experience in these two world-renowned institutes opened my eyes in physics and kept my enthusiastic about the best research. Second, I would also to thank my colleague and mentor Dr. Konstantin Tikhonov, who helped me a lot on clarifying all the conceptual points involved in the project, and guided me through the toughest calculation. I would also like to thank numerous friends in the Physics&Astronomy department of Texas A&M University, with whom I studied physics and enjoyed life. In particular, I would like to thank Mr. Feng Li for the days we spent in self-studying the materials on quantum field theory, which levels up my understanding of physics significantly. Finally, family's support is always so important for me to make me stand on this world. During years of studying physics, my parents has always been supportive and encouraging. Thank you, Mom and Dad! Also, I would like to express my most sincere gratitude to my girlfriend Miss Ting Li, who keep me on the ground and smile towards life when physics pulls hard. I am in debt to her love for my absent due to the traveling. The love brought by my family members keeps me strive for the best in physics. Now, please allow me to dedicate my thesis to you all.

TABLE OF CONTENTS

LIST OF FIGURES

FIGURE Page

1. INTRODUCTION

Graphene – monolayer of graphite – is a fantastic material that leads the world into the literally 2D material age for the first time[1]. Its ultrahigh mobility even in room temperature and many other good properties open many opportunities for device application. Graphene is now really playing a central role in condensed matter physics which connects together various branches of physics.

Transport properties of graphene attract a lot of attention [2] since the very discovery of this fascinating material [1]. It is promising for various applications due to its high charge mobility and unique heat conductivity. Being a real 2D material, graphene has electronic properties that are closely related to its structural properties. Graphene is a truly crystalline membrane, a subject that is extensively studied in soft condensed matter physics in 80's [3]. Due to the famous Mermin–Wagner theorem, a 2D membrane was considered to be inexistent, but it was later found that in crystal membranes the freedom to fluctuate in a third direction and the coupling between in-plane and out of plane strains can stabilize the otherwise unstable membrane [4, 5]. The out of plane fluctuation mode has a quadratic dispersion and is dubbed with a special name: the flexural phonon (FP). Theoretically, it has been realized long ago [6–8] that these transport properties of free-standing (suspended) graphene are strongly influenced by the flexural (out-of-plane) vibrational mode, which deforms the graphene sheet, see Fig. 1.1. From the experimental point of view, the effect of the flexural phonons has been clearly observed in the heat transport [9, 10]. However, it is a more challenging task to identify the effect of the flexural phonons in the electronic transport [11, 12]. This is because the contribution of electron-phonon interaction to the momentum relaxation remains small even at high temperatures, with the main source of the relaxation being elastic impurities [13].

Dephasing rate τ_ϕ^{-1} can be a more suitable quantity for studying the FPs, since static impurities do not cause dephasing. The dephasing rate is usually studied through the phenomenon of the weak localization correction to conductivity [14], an important topic in field of the quantum transport. The physics of the weak localization was investigated thoroughly starting from late 70's [15]. The key point here is that the probability for the quasiparticle to come back to its origin is doubled due to the quantum interference between forward and backward trajectories [16]. The experimental

evidence of this quantum interference comes from the magnetoresistance measurements – a way to destroy the coherence of the quasiparticle by applying external magnetic field. Thus, the dephasing time is of crucial importance in the story, beyond which the interference can not be established. Magnetoresistance measurements are common to detect the dephasing rate in normal disordered conductors as well as in Graphene [17, 18]. Usually the electron-electron interaction [19–22] is considered as the primary mechanism for dephasing. In normal metals dephasing due the phonons are important at a higher temperature. One may expect the same for graphene.

There are two ways [23] for electrons to couple to the ionic degrees of freedom in graphene. First is through the usual deformation potential coupling which induces a scalar potential. It has been realized in the Carbon Nanotube research that, there is another form of coupling between electrons and phonons: vector potential like coupling, which is due to the change in bond length and angle between carbon atoms and thus, hopping amplitude [23]. This kind of coupling is remarkable and ubiquitous. Many interesting new physics can be derived from the induced fictitious gauge field [24]. It even shaped a new subfield in graphene research – the strain engineering [25], for phonons in the long-wavelength limit can be viewed as elastic strain. Upon proper manipulation of the strain experimentalists created pseudo-magnetic field (the name 'pseudo' due to the fact that it still preserve time reversal symmetry) greater than 300 Tesla [26], which generated a lot of new possibilities to observe ubiquitous quantum phenomena without external magnetic field and at a higher temperature, e.g. the zero-field quantum Hall effect [27], Aharonov–Bohm effects from local deformation [28], and also the novel graphene nonelectronic [29].

In my thesis work, we show that the strain induced fictitious gauge field, though preserving time reversal symmetry, would still contribute to dephasing. Thermal fluctuations will easily induce random corrugations or ripples [30] on the graphene sheet and, therefore, random fluctuations of the pseudo-magnetic field. This reminds us about the situation in early 90's when the effect of random static magnetic field in strongly correlated system was heavily investigated [31, 32]. Early study on weak localization of the graphene has mentioned the possible contribution to dephasing from those ripples, which is essentially a kind of static fictitious gauge field. Here we will give a much more quantitative argument on the topic and indicate different effects on various channels.

We will mainly discuss dephasing caused by the electron-flexural phonon (el-FP) interaction in graphene. It is the softness of the flexural mode and the coupling of an electron to two FPs simultaneously (see Fig. 1.2 for illustration) that make the contribution of FPs to τ_ϕ^{-1} in a suspended

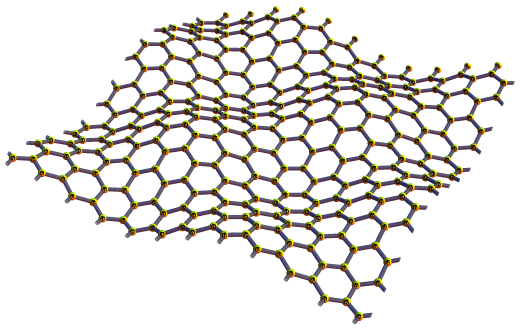

Figure 1.1: Deformation of a graphene sheet. The graphene depicted is under the influence of the out of plane (flexural) vibrational mode.

sample to be significant, and at large enough densities even comparable with the one caused by the electron-electron interaction. Because of the quadratic spectrum of the FP, $\omega_k = \alpha k^2$, FPs are much more populated as compared with the in-plane ones. In addition, the coupling to two FPs considerably increases the phase space available for the inelastic processes as compared to the interaction with a single phonon. The point is that in graphene the Fermi momentum, k_F, is relatively small. As a result, the interaction of a single phonon with electrons is determined by the Bloch-Grüneisen (BG) temperature, $T_{BG} \sim \omega_{2k_F}$, rather than the temperature, when $T \gg T_{BG}$ [33]. In such a case, one needs to exploit other scattering mechanisms to overcome the limitations induced by the smallness of k_F. For example, in supercollisions [34] thermal phonons interact with electrons via impurity scattering which carries away excess momenta. In the case of el-FP interaction, coupling to two phonons radically changes the situation. Now only the transferred momentum should be small, while individually a FP may have a momentum much larger than k_F, up to the thermal momentum q_T.

Still, as we shall demonstrate, the problem of dephasing due to the el-FP interaction appears to be quite special, because the softness of FPs, i.e. unique smallness of T_{BG}, leads to the existence of a temperature range where dephasing rate cannot be obtained using the golden rule (GR), but rather both the self-energy and the vertex processes [35] should be treated simultaneously. This results in a transition from $\tau_\phi^{-1} \sim T^2$ to T with increasing temperature for the dephasing rate induced by FPs.

This thesis is organized as follows: in Sec. 2 we describe the properties flexural phonons, then

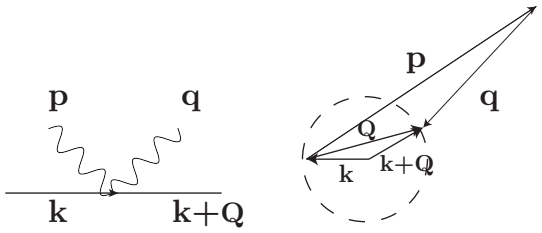

Figure 1.2: Scheme of the el-FP interaction process. On the left, scheme of the el-FP scattering event, where the solid line represents an electron, and the wavy lines represent FPs. On the right, relations among the momenta involved in scattering. FPs can have momenta $\mathbf{p}$, $\mathbf{q}$ much larger than the transferred momentum $\mathbf{Q}$. Under the conditions discussed in the paper, the scattering process is considered as semi-elastic.

in Sec. 3 we review the diagrammatic theory of dephasing and apply it to graphene in Sec. 4, finally we show the phase diagram of the calculate dephasing rate due to the flexural phonons in Sec. 5, discuss the peculiar physics involved in the problem in Sec. 6, followed by a summary as conclusion.

2. FLEXURAL PHONONS AND THEIR FLUCTUATION

In this section we will discuss the properties of flexural phonons (FPs) and their fluctuations.

2.1 Flexural Phonons

The lattice dynamics of the single-layer graphene can be described in terms of the displacement vector $\mathbf{u} = (u_x, u_y, h)$ [3]. Here $u_{x,y}$ describe the in-plane modes, while the out-of-plane displacement h describes the flexural mode. The displacement vector leads to a nonlinear strain tensor of the form

$$u_{ij} = \frac{1}{2}\left(\partial_i u_j + \partial_j u_i + \partial_i h \partial_j h\right), \tag{2.1}$$

where $(i, j) = (x, y)$ are spatial indices. The free energy of the graphene membrane in the harmonic approximation can be expressed as

$$\mathcal{H} = \frac{1}{2}\int d^2x \left(\lambda u_{ii}^2 + 2\mu u_{ij}^2\right) + \frac{\kappa}{2}\int d^2x \left(\nabla^2 h\right)^2,$$

where the first term describes the elastic energy and second one is the bending energy. Here $\kappa \approx 1$eV is the bending rigidity and $\lambda \approx 3$ eV/Å^2, $\mu \approx 9$eV/Å^2 are the in-plane elastic constants. However, simple Levanyuk-Ginzburg criteria [36, 37] arguments show that at $k < q_c(T)$, where $q_c = \frac{\sqrt{T\Delta_c}}{v_F} \approx 0.01\sqrt{T}/\text{Å}$, the harmonic approximation for the flexural mode ceases to work due to anharmonicity. Here $\Delta_c \approx 18.7$eV [8] reflects the energy scale of the anharmonicity. The breakdown of the Gaussian approximation is related to the h^4-vertex, arising as a result of integrating out fast u-modes, which are coupled to h-mode [4, 38] and entering the free energy quadratically. Then, one can immediately see the h^4-vertex from the effective free energy that can be written as

$$\mathcal{H}_{eff} = \frac{\kappa}{2}\int d^2x \left(\nabla^2 h\right)^2 + \frac{1}{8d_c} Y_2 \int \left(d^2x\right)\left(P_{ij}^T \partial_i h \partial_j h\right)^2,$$

where d_c is the codimension [39] and $Y_2 = \frac{4\mu(\mu+\lambda)}{2\mu+\lambda} = 20$eV/Å^2 is the two-dimensional Young's modulus and $P_{ij}^T = \delta_{ij} - \nabla_i \nabla_j / \nabla^2$ is the transverse projector [4]. As a result, the low momentum end of the FP's spectrum is significantly renormalized. This effect can be described by the self-consistent screening approximation (SCSA) theory [39], which includes a partial summation of an infinite series of the h^4-vertex diagrams. While the method is exact in the limit of infinite spatial

dimensions, applying it to a graphene sheet embedded in 3D world is just an extrapolation, where $d_c = 1$. Nevertheless, one can propose the following form of the renormalized spectrum

$$\omega_k = \alpha k^2 \Theta(k), \ \Theta(k) = \sqrt{1 + Z^{-1} (q_c/k)^{\eta}}, \tag{2.2}$$

where $\Theta(k)$ describes a transition from the bare spectrum at high momentum to the renormalized spectrum $\sim k^{2-\eta/2}$ in the low momentum limit. It is important that $1/2 < \eta < 1$. For $\eta > 1/2$, the perturbative calculation for the correlation functions is sufficient. For $\eta < 1$, the FPs remain soft and the integrals determining the correlation functions of the potentials, see Eqs. (2.5) and (2.6) below, converge at small momenta, i.e., $q, p \ll q_T$. The exact Z and η should be extracted from the experiments. Below we will exploit the value $Z \sim 2$, and take $\eta \approx 0.8$ from the numerical solution of the SCSA [40].

2.2 Electron-Flexural Phonon Coupling

There are two ways [23] for electrons to couple with the ionic degrees of freedom. First is through the deformation potential coupling between electrons and acoustic phonons, which can be represented as an effective scalar potential field: $\varphi = g_1 (u_{xx} + u_{yy})$, where $g_1 = 30$eV [23] is the deformation potential constant. Here u_{ij} is the full nonlinear strain tensor. One can then write down the scalar potential due to flexural phonons

$$\varphi = g_1 (f_{xx} + f_{yy})/2,$$

where $f_{ij}(r,t) \equiv \partial_i h \partial_j h$. Another way of coupling is through the changes in bond length and angle in carbon atoms and this induces an fictitious gauge field: $v_F \mathbf{A} = g_2 (u_{xx} - u_{yy}, -2u_{xy})$, where $g_2 = 7.5$eV [23]. Likewise, the fictitious gauge field that is induced by flexural phonons can be written as

$$v_F \mathbf{A} = \frac{g_2}{2} \begin{pmatrix} f_{xx} - f_{yy} \\ -2 f_{xy} \end{pmatrix}.$$

2.3 Fluctuation of the Flexural Phonons

Thermal fluctuations of the lattice produce variations in the potentials. Averaging over lattice vibrations one finds the correlation functions of the potentials as

$$\begin{aligned}\left\langle \varphi\left(\mathbf{Q},\Omega\right)\varphi\left(-\mathbf{Q},-\Omega\right)\right\rangle &= \phi\left(\mathbf{Q},\Omega\right),\\ \left\langle A_i^{\alpha}\left(\mathbf{Q},\Omega\right)A_j^{\beta}\left(-\mathbf{Q},-\Omega\right)\right\rangle &= s^{\alpha}s^{\beta}\mathcal{A}_{ij}\left(\mathbf{Q},\Omega\right).\end{aligned} \tag{2.3}$$

where we define the thermal average $\langle ...\rangle \equiv Z^{-1}Tr\left[...\exp\left(-\beta\mathcal{H}_{eff}\right)\right]$, here $\beta = 1/T$ is the inverse temperature. To proceed, we introduce the correlation function for FP

$$\left\langle h\left(\mathbf{k},\omega\right)h\left(-\mathbf{k},-\omega\right)\right\rangle \equiv H\left(k\right)2\pi\delta\left(\omega-\omega_k\right), \tag{2.4}$$

where $H\left(k\right)$ can be found from the action describing the elastic deformation of graphene.

In the harmonic approximation, $H\left(k\right) = \frac{n(\omega_k)}{\rho\omega_k}$, where $n\left(\omega\right)$ is the Planck distribution function and ρ is the mass density of the graphene sheet.

Combining the equations above, we obtain for the scalar potential correlation function

$$\begin{aligned}\phi\left(\mathbf{Q},\Omega\right) =& \frac{1}{8}g_1^2\left(Q\right)\int\left(d^2\mathbf{p}\right)\left(d^2\mathbf{q}\right)\left[\mathbf{p}\cdot\mathbf{q}\right]^2\\ &\times H\left(p\right)H\left(q\right)\delta_{\mathbf{p},\mathbf{q}}\left(\Omega,\mathbf{Q}\right),\end{aligned} \tag{2.5}$$

where $\delta_{\mathbf{p},\mathbf{q}}\left(\Omega,\mathbf{Q}\right) \equiv \sum_{\pm}\left(2\pi\right)^3\delta\left(\Omega\pm\omega_{\mathbf{p}}\pm\omega_{\mathbf{q}}\right)\times\ \delta\left(\mathbf{Q}-\mathbf{p}-\mathbf{q}\right)$, and $\omega_{\mathbf{p},\mathbf{q}}$ are given by Eq. (2.2). Here the summation includes four different processes of emission/absorption of two FPs by an electron. Since each time an electron is coupled to *two* flexural phonons, ϕ describes a phonon loop and, therefore, in the momentum-frequency domain $\phi\left(\mathbf{Q},\Omega\right)$ has a extended support rather than a δ-function peak. Same as the scalar counterpart, we can get for the vector potential correlation function

$$\begin{aligned}\mathcal{A}_{ij}\left(\mathbf{Q},\Omega\right) =& \frac{\hat{\mathbf{n}}_i\hat{\mathbf{n}}_j}{8}\left(g_2/v_F\right)^2\int\left(d^2\mathbf{p}\right)\left(d^2\mathbf{q}\right)p^2q^2\\ &\times H\left(p\right)H\left(q\right)\delta_{\mathbf{p},\mathbf{q}}\left(\Omega,\mathbf{Q}\right),\end{aligned} \tag{2.6}$$

where $\hat{\mathbf{n}} = \left(\cos 2\hat{Q}, -\sin 2\hat{Q}\right)$.

2.4 Screening due to Electrons

We briefly discuss the problem of screening. The deformation potential constant represents the coupling of ions to electron density, therefore the coupling constant will be screened by the electron-hole polarization operator as in ordinary metals. It reduces to a Thomas-Fermi like expression

$$g_1^{'}(Q) = g_1/\epsilon(Q) = g_1 \frac{Q}{Q+\varkappa}$$

where $\varkappa = g_e N k_F$, $N = 4$ is the spin-valley degeneracy in graphene, and $g_e \sim 1$ describes the renormalized Coulomb interaction [41]. Moreover, the polarization bubble of the flexural phonons also suffers from the screening by itself due to the second term in $\mathcal{H}_{eff}$. This effect is included by a partial summation of infinite amount of vertex renomalization diagrams [39, 42], i.e., by using the renormalized spectrum employing SCSA, Eq. (2.2).

3. THE THEORY OF DEPHASING

Main tool to probe electronic coherence is magnetoresistance [43], which gives a direct access to the weak localization corrections to conductivity, controlled by the dephasing rate τ_ϕ^{-1}. The weak localization correction to conductivity in graphene can be written as [44, 45]

$$\Delta\sigma = -\frac{2e^2 D}{\pi} \sum_l \int dt C^l \left(-t/2, t/2\right), \tag{3.1}$$

where l sums over four Cooperon channels relevant for the magnetoresistance. Physically, $C^l\left(-t/2, t/2\right)$ represents the interference of a pair of time reversed trajectories in the channel l that start at $-t/2$ and return to the initial point at $t/2$. More generally, the Cooperon matrix $C^{l_1 l_2}_{s_1 s_2}$ is labeled by two isospin numbers $s_{1,2}$ and two pseudospin numbers $l_{1,2}$. It is diagonal in the pseudospin space even in the presence of interactions that preserve sublattice and valley indices. The Cooperon channels relevant for magnetoresistance are the isospin singlets, $C^l \equiv C^{ll}_{00}$ $(l = 0, x, y, z)$, whose gaps are small compared with τ^{-1}, the elastic scattering rate due to impurities. Therefore, we restrict ourselves to this subspace.

3.1 Diagrammatic Calculation of the Decay Function

To include el-FP interaction into the Cooperon, one can write down a Bethe-Salpeter equation for a particular Cooperon channel C^l. In the following we will not solve the equation exactly, but instead, we will estimate the upper bound of the Cooperon decay rate [46, 47]. We start by writing down an ansatz that reads as [35]

$$C^l\left(t_1, t_2\right) = C_0^l\left(t_1 - t_2\right) e^{-F^l\left(t_1, t_2\right)}. \tag{3.2}$$

Here $C_0^l\left(t\right)$ is the diffusion propagator describing the bare Cooperon, and $F^l\left(t_1, t_2\right)$ is a decay function characterizing the effect of the el-FP interaction. To the lowest order in the interaction propagators, the expression for F^l can be obtained as

$$F^l\left(t_1, t_2\right) \simeq -\frac{C_1^l\left(t_1, t_2\right)}{C_0^l\left(t_1 - t_2\right)}, \tag{3.3}$$

where C_1^l is the first order correction to the Cooperon in terms of the interactions propagators, see Fig. 3.1.

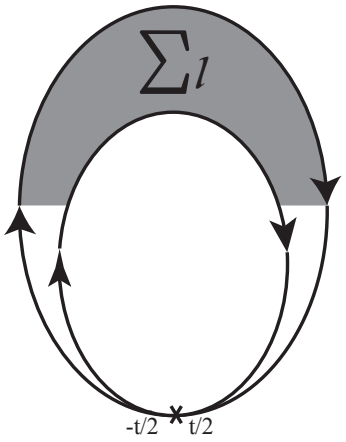

Figure 3.1: Diagramatic representation of the decay function $F(t)$. Here $\Sigma_l = \Sigma_l^{self} + \Sigma_l^{vert}$.

For each channel, the contribution of the el-FP interaction can be separated into the scalar and vector potential ones. Also, the effect of the interaction is separated into the self-energy and vertex (vertical) contributions, denoted as $\Sigma^{self/vert}$; see Fig. 3.2. Thus, one can write $F^l = F_\phi^l + F_A^l$, and $\Sigma^{l,self/vert} = \Sigma_\phi^{l,self/vert} + \Sigma_A^{l,self/vert}$. We concentrate first on dephasing caused by the scalar potential fluctuation $\phi(\mathbf{Q}, \Omega)$. The calculation for the vector potential contribution goes along the similar lines, and results are presented in the end of this Section.

3.1.1 Scalar Potential Coupling

In Eq. (3.8), the Cooperon variables $(\tilde{q}, \tilde{\omega})$ are small comparing to the electronic scales determining the el-FP interaction process, i.e., $\tilde{q} \ll k_F$ and $\tilde{\omega} \ll \mu$. Therefore, one can drop out $(\tilde{q}, \tilde{\omega})$ dependences from the interaction propagators Σ. Furthermore, as far as $T \gg T_{BG}$, the typical momentum transfer $Q \sim 2k_F \gg 1/v_F\tau$. Therefore, dephasing can be calculated assuming that electron's motion during the interaction event is ballistic.

The self-energy and vertex contribution of the channel l are defined in the iso-pseduospin basis via $\Sigma^{l,self/vert} \equiv (\Sigma_y \Lambda_y \Lambda_l)_{\alpha\beta} \Sigma_{\alpha\beta;\gamma\delta}^{self/vert,} (\Sigma_y \Lambda_l \Lambda_y)_{\delta\gamma}$ (summation for Greek letters is implied; indices

$\phi(A)$ are omitted). Here, the self-energy contribution, see Fig. 3.2(a), can be written as

$$\tau\Sigma^{self,\phi}_{\alpha\beta;\gamma\delta,}(\tilde{q},Q,\tilde{\omega},\Omega)=-\frac{g(Q)^2}{\pi\nu_0\tau}\int\left(d^2p\right)\left(-\frac{i}{2}D^K(Q,\Omega)\right)\times$$
$$\{\left[G^R\left(p^+,E^+\right)G^R\left(p^+-Q,E^+-\Omega\right)G^R\left(p^+,E^+\right)\right]_{\alpha\beta}G^A\left(p^-,E^-\right)_{\gamma\delta}$$
$$+G^R\left(p^+,E^+\right)_{\alpha\beta}\left[G^A\left(p^-,E^-\right)G^A\left(p^--Q,E^--\Omega\right)G^A\left(p^-,E^-\right)\right]_{\gamma\delta}\},\quad(3.4)$$

where $E^{\pm}=\mu\pm\tilde{\omega}/2$, $p^{\pm}=k_F\pm\tilde{q}/2$. Note that arguments $\tilde{q}$ and $\tilde{\omega}$ are related to the propagation of the Cooperon, while Q and Ω describe the interactions with FPs causing the dephasing. The vertex contribution, see Fig. 3.2(b), is

$$\tau\Sigma^{vert,\phi}_{\alpha\beta;\gamma\delta}(\tilde{q},Q,\tilde{\omega},\Omega)=-\frac{g(Q)^2}{\pi\nu_0\tau}\int\left(d^2p\right)\left(-\frac{i}{2}D^K(Q,\Omega)\right)\times$$
$$\left[G^R\left(p^+,\varepsilon^+-\Omega\right)G^R\left(p^++Q,\varepsilon^+\right)\right]_{\alpha\beta}\left[G^A\left(p^-,\varepsilon^-+\Omega\right)G^A\left(p^--Q,\varepsilon^-\right)\right]_{\gamma\delta},\quad(3.5)$$

where $\varepsilon^{\pm}=E^{\pm}\pm\Omega/2$.

Due to the softness of FPs, the integrals in Eq. (3.8) converge at small frequencies $\Omega\ll T$. Therefore, when calculating the effect of interaction on the Cooperon propagators, one may keep only the classical (Keldysh) component of the interaction, $D^K_\phi(\mathbf{Q},\Omega)=-2i\phi(\mathbf{Q},\Omega)$, and send $n(\omega_k)$ in $H(k)$ to its classical limit, $\frac{T}{\omega_k}$. If the full quantum problem is considered, one needs to use $\frac{1}{\sinh(\omega_k/T)}$, in order to incorporate Pauli principle due the presence of other electrons [47]. This leads to the same result for $T\gg\omega_k$, but ensures that quantum fluctuations do not lead to dephasing at zero temperature. Note that the assumption that $\Omega\ll T$ depends crucially on the fact that $\tau_\phi^{-1}\ll T$ which has been checked a posteriori. After a simple calculation, one concludes for scalar potential

$$\Sigma^{l,self}_\phi=-\Sigma^{l,vert}_\phi=\Sigma_\phi(Q,\Omega),\quad(3.6)$$

where $\Sigma_\phi(Q,\Omega)\equiv\phi(\mathbf{Q},\Omega)\mathcal{B}_\phi(Q)$. Here,

$$\mathcal{B}(\mathbf{Q})=\frac{2}{v_FQ}\left(1-(Q/2k_F)^2\right)^{1/2}\theta(2k_F-Q),\quad(3.7)$$

where the Heaviside theta function $\theta(2k_F-Q)$ restricts the momentum that can be exchanged

between FPs and electrons. This leads to

$$C_1^l(t_1,t_2) = \int (dQ)(d\Omega)(d\tilde{q})(d\tilde{\omega})\, e^{-i\tilde{\omega}t_{12}}[C_0^l(\tilde{q},\tilde{\omega})\,\Sigma_{Q,\tilde{q}}^{l,self}(\tilde{\omega},\Omega)\,C_0^l(\tilde{q},\tilde{\omega}) + e^{i\Omega\tau_{12}}C_0^l(\tilde{q},\tilde{\omega}-\Omega)\,\Sigma_{Q,\tilde{q}}^{l,vert}(\tilde{\omega},\Omega)\,C_0^l(\tilde{q},\tilde{\omega}+\Omega)], \tag{3.8}$$

where $t_{12} = t_1 - t_2$ and $\tau_{12} = t_1 + t_2$.

As a result, the decay function for the scalar potential $F_\phi(t)$ is the same for all channels, and it can be expressed as a convolution of three factors: i) the correlation function $\phi(\mathbf{Q},\Omega)$, ii) function $\mathcal{B}(k)$, describing the ballistic electron's motion, and iii) factor $\mathcal{C}^\phi(\Omega,t)$, reflecting the relation between the self-energy and vertex diagrams:

$$F_\phi(t) = t\int (d\mathbf{Q})(d\Omega)\,\phi(\mathbf{Q},\Omega)\,\mathcal{B}(\mathbf{Q})\,\mathcal{C}^\phi(\Omega,t)\,. \tag{3.9}$$

The factor $\mathcal{C}^\phi(\Omega,t)$ is obtained by performing the $(\tilde{q},\tilde{\omega})$ integration in Eq. (3.8), and is equal to

$$\mathcal{C}^\phi(\Omega,t) = 1 - \frac{\sin\Omega t}{\Omega t}. \tag{3.10}$$

3.1.2 Vector Potential Coupling

In the case of vector potential coupling, one calculates a diagram similar to that in Fig. 3.2, and gets

$$\Sigma_A^{l,self} = s_l\Sigma_A^{l,vert} = \Sigma_A^{ij}(Q,\Omega)\,\delta_T^{ij}(Q)\,, \tag{3.11}$$

where $\delta_T^{ij}(Q) = \delta^{ij} - Q^iQ^j/Q^2$ and $\Sigma_A^{ij}(Q,\Omega) = v_F^2\mathcal{A}^{ij}(\mathbf{Q},\Omega)\,\mathcal{B}_A(Q)$. Here, $\mathcal{A}^{ij}(\mathbf{Q},\Omega)$ is defined in Eq. (2.6), and

$$\mathcal{B}_A(Q) = \frac{2}{v_FQ}\left(1-(Q/2k_F)^2\right)^{-1/2}\theta(2k_F-Q)\,. \tag{3.12}$$

The corresponding decay function can be rendered as (compare with Eq. (3.9))

$$F_A^l(t) = t\int (d\mathbf{Q})(d\Omega)\,v_F^2\mathcal{A}^{ij}(\mathbf{Q},\Omega)\,\delta_T^{ij}(Q)\,\mathcal{B}_A(Q)\,\mathcal{C}_l^A(\Omega,t)\,, \tag{3.13}$$

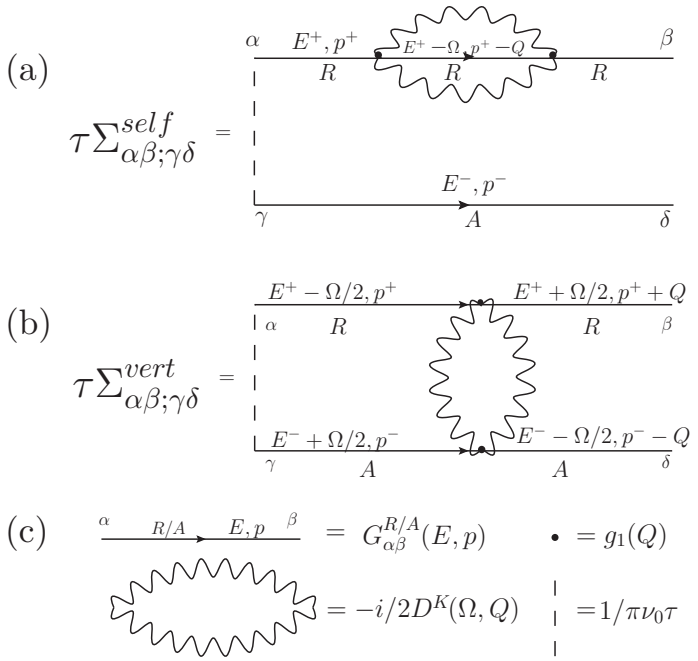

Figure 3.2: Diagrammatic representation of the self-energy and vertex Contributions. (a) The self-energy contribution, (b) the vertex contribution and, (c) diagrammatic dictionary for the various objects involved: $E^{\pm} = \mu \pm \tilde{\omega}/2$ and $p^{\pm} = k_F \pm \tilde{q}/2$; ν_0 is the density of states at Fermi energy, and $g_1(Q)$ is the coupling constant with screening included.

where

$$\mathcal{C}_l^A(\Omega, t) = 1 + s_l \frac{\sin \Omega t}{\Omega t}. \tag{3.14}$$

The intervalley Cooperons are coupled to the vector potential field of the opposite signs. Thus, $s_l = \pm 1$ for intra-/intervalley Cooperons. Further on, one can resolve the transverse delta function δ_T^{ij} and get

$$F_A^l(t) = t \int \sin^3 \hat{Q} \, (d\mathbf{Q}) \, (d\Omega) \, \mathcal{A}(\mathbf{Q}, \Omega) \, \mathcal{B}_A(Q) \, \mathcal{C}_l^A(\Omega, t), \tag{3.15}$$

where

$$\mathcal{A}(\mathbf{Q}, \Omega) = \frac{g_2^2}{8} \int \left(d^2\mathbf{p}\right) \left(d^2\mathbf{q}\right) p^2 q^2 H(\mathbf{p}) \, H(\mathbf{q}) \, \delta_{\mathbf{p},\mathbf{q}}(\Omega, \mathbf{Q}). \tag{3.16}$$

Here $\delta_{\mathbf{p},\mathbf{q}}(\Omega, \mathbf{Q}) = \sum_{\pm} (2\pi)^3 \delta(\Omega \pm \omega_{\mathbf{p}} \pm \omega_{\mathbf{q}}) \, \delta(\mathbf{Q} - \mathbf{p} - \mathbf{q})$ and the summation includes four different processes of emission/absorption of two FPs by an electron.

4. DEPHASING RATE DUE TO THE FLEXURAL PHONONS

In this section we will apply the theory discussed in Section 3 to deal with the problem of dephasing due to the electron-flexural phonon interactions. We will discuss both scalar and vector potential coupling.

4.1 The Decay Function

4.1.1 Scalar Potential Coupling

The dephasing rate τ_ϕ^{-1} is defined according to $F_\phi(\tau_\phi) = 1$. The decay function can be most conveniently expressed as

$$F_\phi(t) = c_\phi^2 t T f(\mathcal{T}, \xi) \frac{T}{\mu}, \tag{4.1}$$

where $c_\phi = \frac{g_1/\rho\alpha^2}{2\pi g_e N} \sim 1.2$ is dimensionless coupling constant and f is a dimensionless function of two parameters: $\mathcal{T} = \alpha k_F^2 t$ and $\xi = Z^{-1/\eta} q_c/k_F$. Parameter ξ originates from the renormalization of the FP spectrum described by Θ in Eq. (2.2); $\Theta(k_F) = \sqrt{1+\xi^\eta}$.

Let us now evaluate the integral in Eq. (2.5) explicitly. It is convenient to use the time representation for the energy delta-function:

$$\sum_{\pm} (2\pi)\,\delta(\Omega \pm \omega_{\mathbf{p}} \pm \omega_{\mathbf{q}}) = 4\int d\tau \cos(\omega_p \tau)\cos(\omega_q \tau)\exp[-i\Omega\tau]. \tag{4.2}$$

After this, one can integrate Eq. (3.9) in frequency Ω, using

$$\int (d\Omega)\, e^{-i\Omega\tau}\left(1 - \frac{\sin\Omega t}{\Omega t}\right) = \frac{1}{t}\Xi_-(\tau/t), \tag{4.3}$$

where

$$\Xi_\pm(s) \equiv \delta(s) \pm \frac{1}{2}\theta(1-|s|). \tag{4.4}$$

The next step is to make the integral dimensionless by introducing $\tau = st$ and dimensionless 2D vectors $\mathbf{x}, \mathbf{y}, \mathbf{z} = \mathbf{p}/k_F, \mathbf{q}/k_F, \mathbf{Q}/k_F$. Using the expression for $H(q)$ in the classical limit, $H(q) = \frac{T}{\rho\omega_q^2}$ (ω_q is defined in Eq. (2.2)), we obtain the decay function as given in Eq. (4.1)

$$F_\phi(t) = c_\phi^2 t T f_\phi\left(\alpha k_F^2 t, Z^{-1/\eta} q_c/k_F\right)\frac{T}{\mu}. \tag{4.5}$$

Here,

$$f_\phi(\mathcal{T},\xi)=4\pi^2\int(2\pi)^2(d\mathbf{z})(d\mathbf{x})(d\mathbf{y})\,\delta(\mathbf{z}-\mathbf{x}-\mathbf{y})\,S(z)\,\frac{(\mathbf{x}\cdot\mathbf{y})^2}{x^4y^4}$$
$$\int\Xi_-(s)\,ds\frac{\cos\left(\mathcal{T}sx^2\Theta_\xi(x)\right)\cos\left(\mathcal{T}sy^2\Theta_\xi(y)\right)}{\Theta_\xi^2(x)\,\Theta_\xi^2(y)} \tag{4.6}$$

with $\mathcal{T}=\alpha k_F^2 t$, $\xi=Z^{-1/\eta}q_c/k_F$, $\Theta_\xi(x)=\sqrt{1+(x/\xi)^{-\eta}}$, and

$$S_\phi(z)=\left(\frac{z}{1+z/(g_eN)}\right)^2\sqrt{1-(z/2)^2}\theta(2-z), \tag{4.7}$$

which is the product of the screening and chiral factors. Here $N=4$ is the spin-valley degeneracy in graphene, and g_e describes the renormalized Coulomb interaction.

To proceed, it is convenient to make some transformations in Eq. (4.6). First, we integrate out s exactly, using the relation

$$\int\Xi_\pm(s)\,ds\cos(sa)\cos(sb)=\Xi_\pm(a,b), \tag{4.8}$$

with

$$\Xi_\pm[a,b]=1\pm\frac{a\sin a\cos b-b\sin b\cos a}{a^2-b^2}. \tag{4.9}$$

This gives

$$f_\phi(\mathcal{T},\xi)=(2\pi)^4\int(d\mathbf{z})(d\mathbf{x})(d\mathbf{y})\,\delta(\mathbf{z}-\mathbf{x}-\mathbf{y})\,S_\phi(z)\,\frac{(\mathbf{x}\cdot\mathbf{y})^2}{x^4y^4}\frac{\Xi_-\left[\mathcal{T}\Theta_\xi(x)\,x^2s,\mathcal{T}\Theta_\xi(y)\,y^2s\right]}{\Theta_\xi^2(x)\,\Theta_\xi^2(y)}. \tag{4.10}$$

The final step is to resolve the delta-function in the above expression for $\mathbf{y}$ which yields

$$y=\sqrt{z^2+x^2-2zx\cos\psi}, \tag{4.11}$$

where ψ is the angle between $\mathbf{z}$ and $\mathbf{x}$. As a result, one finally obtains

$$f_\phi(\mathcal{T},\xi)=\int_0^2 dzS_\phi(z)\int_0^\infty dx\int_0^{2\pi}\frac{d\psi}{2\pi}\frac{(z\cos\psi-x)^2}{xy^4}\frac{\Xi_-\left[\mathcal{T}\Theta_\xi(x)\,x^2,\mathcal{T}\Theta_\xi(y)\,y^2\right]}{\Theta_\xi^2(x)\,\Theta_\xi^2(y)}, \tag{4.12}$$

4.1.2 Vector Potential Coupling

We define

$$F_A^l(t) \equiv c_A^2 t T f_A^l\left(\alpha k_F^2 t, Z^{-1/\eta} q_c/k_F\right)\frac{T}{\mu}, \tag{4.13}$$

where c_A is the dimensionless el-FP coupling constant for the vector potential.

4.1.2.1 Intervalley Channels ($l = 0, z$)

Since $s_l = -1$, the decay function for the intervalley Cooperons is similar with that for the scalar potential. Without providing further details, we conclude that

$$f_A^l(\mathcal{T},\xi) = \int_0^2 dz S_A(z)\int_0^\infty dx\int_0^{2\pi}\frac{d\psi}{2\pi}\frac{1}{xy^2}\frac{\Xi_-\left[\mathcal{T}\Theta_\xi(x)x^2, \mathcal{T}\Theta_\xi(y)y^2\right]}{\Theta_\xi^2(x)\Theta_\xi^2(y)}, \tag{4.14}$$

where y has been defined by Eq. (4.11), and

$$S_A(z) = \frac{1}{2}\left(1-(z/2)^2\right)^{-1/2}\theta(2-z). \tag{4.15}$$

Note that $S_A(z)$ includes only the chiral factor since screening does not affect the vector potential coupling constant.

4.1.2.2 Intravalley Channels ($l = x, y$)

For the intravalley channels, $s_l = 1$. Correspondingly Ξ_- has to be changed to Ξ_+:

$$f_A^l(\mathcal{T},\xi) = \int_0^2 dz S_A(z)\int_0^\infty dx\int_0^{2\pi}\frac{d\psi}{2\pi}\frac{1}{xy^2}\frac{\Xi_+\left[\mathcal{T}\Theta_\xi(x)x^2, \mathcal{T}\Theta_\xi(y)y^2\right]}{\Theta_\xi^2(x)\Theta_\xi^2(y)}. \tag{4.16}$$

4.2 Asymptotic Properties of the Decay Function

The analytical expressions obtained in the previous sections allow us to determine $\tau_{\phi/A}$ at arbitrary temperature T and chemical potential μ. (In the end, the dephasing times $\tau_{\phi/A}$ are defined as solution of the equations $F_{\phi/A}\left(\tau_{\phi/A}\right) = 1$.) We have developed numerical procedure, which exploits these equations to calculate corresponding $\tau_\phi(T,\mu)$ dependencies. Before presenting general results, let us concentrate on the properties of the functions $f_{\phi/A}(\mathcal{T},\xi)$ in the analytically accessible regimes.

4.2.1 Scalar Potential Coupling

4.2.1.1 Large ξ

For $\xi \gg 1$, one may identify three asymptotic regions depending on $\mathcal{T}$. When $\mathcal{T} \ll \xi^{-2}$, the integral in $f_\phi(\mathcal{T},\xi)$ is dominated by the quadratic spectrum where $\Theta_\xi(x) = 1$ (refer to Eq. (4.12)), while at $\xi^{-2} \ll \mathcal{T} \ll \xi^{-\eta/2}$ the integral is dominated by the part of spectrum where $\Theta_\xi(x) = (x/\xi)^{-\eta/2}$. Thus, for not too large $\mathcal{T}$ $\left(\mathcal{T} \ll \xi^{-\eta/2}\right)$, one may assume that the spectrum is homogenous, and put $\Theta_\xi(x) = (x/\xi)^b$. Then the function f_ϕ reads:

$$f_\phi(\mathcal{T},\xi) = \frac{\xi^{4b}}{2\pi}\int_0^2 dz S_\phi(z)\int_0^\infty dx\int_0^{2\pi} d\psi \frac{(z\cos\psi - x)^2}{x^{1+2b}y^{4+2b}}\Xi_-\left[\mathcal{T}(x/\xi)^b x^2, \mathcal{T}(y/\xi)^b y^2\right]. \quad (4.17)$$

We obtain,

$$f_\phi(\mathcal{T},\xi) = c(b)\,\xi^{\frac{6b}{2+b}}\mathcal{T}^{\frac{2+4b}{2+b}}, \quad (4.18)$$

with $c(b) = \frac{M_b N_\phi}{2+b}$, where $N_\phi = \int_0^2 dz S_\phi(z) = 0.89$ (assuming $g_e \approx 1$), and

$$M_b = \int_0^\infty u^{-\frac{5b+4}{b+2}}\Xi_-(u,u)\,du = 2^{\frac{3b}{b+2}}\Gamma\left(-\frac{5b+4}{b+2}\right)\sin\frac{(5b+4)\pi}{(b+2)2}. \quad (4.19)$$

More specifically, for $b = -\eta/2$, $c_I^\eta \equiv c(-\eta/2) = 0.03$, when $\eta = 0.8$. For $b = 0$, $c_{II} \equiv c(0) = \frac{\pi}{8}N_\phi$. The scaling expression in Eq. (4.18) can be achieved due to the fact that one can neglect all the z dependences except for $S_\phi(z)$ in Eq. (4.17). Then, $y \simeq x$, ψ integral gives 2π, and the remaining integral over x leads to Eq. (4.18). The obtained asymptotes will describe non-golden rule behavior for the decay function, in the region I ($b = -\eta/2$) and II ($b = 0$). Note that for $b = 0$, $f_\phi = c_{II}\mathcal{T}$.

Next, for $\mathcal{T} \gg \xi^{-\eta/2}$, the golden rule regime holds and the vertex diagram is not important anymore. In this case, one can put $\Xi_- \to 1$, and $f_\phi(\mathcal{T},\xi)$ becomes independent on $\mathcal{T}$:

$$\begin{aligned} f_\phi(\mathcal{T},\xi) &= \int_0^2 dz S_\phi(z)\int_0^\infty dx\int_0^{2\pi}\frac{d\psi}{2\pi}\frac{(z\cos\psi - x)^2}{xy^4}\frac{1}{\Theta_\xi^2(x)\,\Theta_\xi^2(y)} \\ &= c_{IV}^\eta \xi^{-2\eta}, \end{aligned} \quad (4.20)$$

where $c_{IV}^\eta = \eta U^\eta W^\eta \int_0^2 dz S_\phi(z) z^{2\eta-2}$. Here, with $J_n(u)$ being the Bessel function of the first kind, $U^\eta \equiv \int_0^\infty u^{-2\eta}J_1(u)\,du = \frac{4^{-\eta}\Gamma(1-\eta)}{\Gamma(1+\eta)}$, and $W^\eta \equiv \left(\int_0^\infty u^{\eta-1}J_0(u)\,du\right)^2 + \left(\int_0^\infty u^{\eta-1}J_2(u)\,du\right)^2 = \left(\frac{2^{\eta-1}\Gamma(\eta/2)}{\Gamma(1-\eta/2)}\right)^2 + \left(\frac{2^{\eta-1}\Gamma(1+\eta/2)}{\Gamma(2-\eta/2)}\right)^2$. For $\eta = 0.8$, this yields $U^\eta = 1.63$ and $W^\eta = 2.42$. Eq. (4.20)

describes the asymptotic behavior of the function $f_\phi(\mathcal{T},\xi)$ in region IV.

As a result, we see that the function $f_\phi(\mathcal{T},\xi)$ for large ξ evolves with growing $\mathcal{T}$ as follows (regions of applicability can be easily read off from these equations):

$$c_{II}\mathcal{T} \to c_I^\eta \xi^{-\frac{3\eta}{2-\eta/2}} \mathcal{T}^{\frac{2-2\eta}{2-\eta/2}} \to c_{IV}^\eta \xi^{-2\eta}. \tag{4.21}$$

As indicated in the main text, the matching of different asymptotes gives us a separation between different regions of the dephasing rate on the $(T-\mu)$ plane: The black line in the Fig. (4m) corresponds to matching of the first pair of asymptotes. The location of the region IV is related to matching of the second pair.

4.2.1.2 Small ξ

For small $\xi \ll 1$, there are two asymptotic regions depending on the value of $\mathcal{T}$. For $\mathcal{T} \ll 1$, the integral in Eq. (4.17) is always dominated by the quadratic spectrum ($b=0$), and function $f_\phi(\mathcal{T},\xi)$ acquires the asymptote linear in $\mathcal{T}$ (compare with Eq. (4.18) at $b=0$):

$$f_\phi(\mathcal{T},\xi) = c_{II}\mathcal{T}. \tag{4.22}$$

At large $\mathcal{T} \gg 1$, the golden rule is applicable. In this region,

$$f_\phi(\mathcal{T},\xi) = c_{III}\log 1/\xi, \tag{4.23}$$

where $c_{III} = \int_0^2 S_\phi(z)/z^2 dz$. Note, that c_I^η, c_{II}, c_{III} and c_{IV}^η implicitly depend on g_e via $S_\phi(z)$, see Eq. (4.7). Thus, in the case of small ξ, $f_\phi(\mathcal{T},\xi)$ evolves with growing $\mathcal{T}$ as follows

$$c_{II}\mathcal{T} \to c_{III}\log 1/\xi. \tag{4.24}$$

The blue line in the Fig. (4m) corresponds to matching of the above asymptotes.

Equation (4.12) allows for straightforward numerical evaluation. Here as an illustration, we present the numerical calculation of the function $f_\phi(\mathcal{T})$. From the plot we see an excellent agreement with theoretical calculation for the region $\mathcal{T} \ll 1$ and $\mathcal{T} \gg 1$, even for an intermediate value of $\xi = 0.52$.

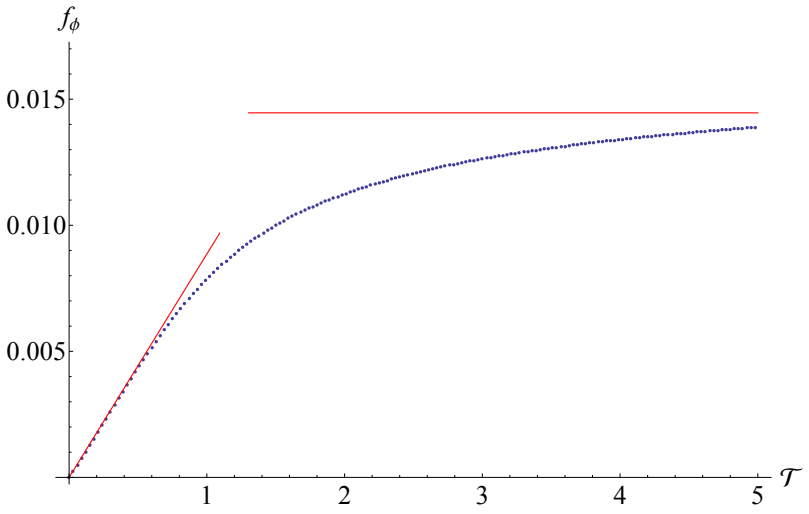

Figure 4.1: Plot of the function $f_\phi(\mathcal{T})$. The parameters are taken as follows: $\eta = 0.8$, $\xi = 0.52$, and $Z = 3$. The blue dots are numerical calculation and the red lines are the asymptotes for different region mentioned above.

4.2.2 Vector Potential Coupling

4.2.2.1 Intervalley Channel

The similarity (compare Eq. (4.12) with Eq. (4.14)) with the scalar potential case makes the calculation of asymptotes for the function $f_A^l(\mathcal{T},\xi)$ straightforward. The function $f_A^l(\mathcal{T},\xi)$ evolves with the growth of $\mathcal{T}$ in the following fashion: for $\xi \gg 1$,

$$d_{II}\mathcal{T} \to d_I^\eta \xi^{-\frac{3\eta}{2-\eta/2}} \mathcal{T}^{\frac{2-2\eta}{2-\eta/2}} \to d_{IV}^\eta \xi^{-2\eta}; \tag{4.25}$$

while for $\xi \ll 1$,

$$d_{II}\mathcal{T} \to d_{III}\xi^{-1}. \tag{4.26}$$

Note that due to the absence of screening, dependence on ξ is stronger than in the case of the scalar potential, compare Eq. (4.24) with Eq. (4.26).

Let us present some technical details. Here $d_I^\eta \equiv d(-\eta/2)$, where $d(b) = \frac{\pi}{4}\frac{M_b}{1+b/2}$ and M_b is defined in Eq. (4.19); specifically, for $b = 0$, $d_{II} \equiv d(0) = 1/64$. In the GR region, the function

$f_A^l(\mathcal{T},\xi)$ is independent on $\mathcal{T}$. Its asymptotic behavior is given as follows:

$$f_A(\xi) = \int_0^2 dz S_A(z) \int_0^\infty dx \int_0^{2\pi} \frac{d\psi}{2\pi} \frac{1}{xy^2} \frac{1}{\Theta_\xi^2(x)\Theta_\xi^2(y)}$$
$$\equiv \begin{cases} d_{III}\xi^{-1} & \text{for} \quad \xi \ll 1 \\ d_{IV}^\eta \xi^{-2\eta} & \text{for} \quad \xi \gg 1 \end{cases}. \tag{4.27}$$

Here, for $\eta > 1/2$ (It is important for the convergence of the following integral.),

$$d_{III} = \frac{1}{2}\int_0^\infty dz \int_0^\infty dx \int_0^{2\pi} \frac{d\psi}{2\pi} \frac{1}{xy^2} \frac{1}{\Theta_{\xi=1}^2(x)\Theta_{\xi=1}^2(y)}, \tag{4.28}$$

and

$$d_{IV}^\eta = 2\eta U^\eta V^\eta G_A, \tag{4.29}$$

where U^η is the same as in the case of the scalar potential, $V^\eta \equiv \left(\int_0^\infty u^{\eta-1} J_0(u)\, du\right)^2 = \left(\frac{2^{\eta-1}\Gamma(\eta/2)}{\Gamma(1-\eta/2)}\right)^2$ and $G_A = \int_0^2 dz S_A(z) z^{2\eta-2} = \frac{4^\eta\sqrt{\pi}}{8}\frac{\Gamma(\eta-1/2)}{\Gamma(\eta)}$. For $\eta = 0.8$, this yields $V^\eta = 1.68$ and $G_A = 1.73$.

4.2.2.2 Intravalley channel

For the intravalley Cooperon, the function $f_A^l(\mathcal{T},\xi)$ involves Ξ_+ which does not vanish in the limit of $\mathcal{T} \to 0$. Therefore, it evolves with the growth of $\mathcal{T}$ (i.e., from $\mathcal{T} \ll 1$ to $\mathcal{T} \gg 1$) as

$$2f_A(\xi) \to f_A(\xi), \tag{4.30}$$

where $f_A(\xi)$ is defined in Eq. (4.27). Note that for the intravalley channels the diffusive limit ($q_c l \ll 1$) for the calculation of dephasing due to the el-FP interaction can be achieved at higher temperature as compared to the intervalley channels. For example, for $g_\square \sim 10$ and $\mu \sim 0.1$eV, the diffusive limit occurs already below $T \sim 0.5$K.

5. PHASE DIAGRAM OF THE DEPHASING RATE

The results are illustrated with the help of Fig. 5.1, where regions I, II and III with a different dephasing rate behavior are indicated in the $(T-\mu)$ plane. The regions are divided in accord with the importance of the renormalized spectrum of the FP and the relative contributions of the self-energy and vertex diagrams. In region I, which is on the left of the black line (i.e., at small densities), the characteristic momenta of p and q in Eq. (2.5) do not exceed q_c. Therefore, the renormalization of the FP spectrum is important, and $\omega_q \sim q^{2-\eta/2}$ should be used. In region II, since the characteristic momenta of the FPs are larger than q_c, it suffices to use the quadratic spectrum for FPs. In region III, which is in the bottom part below the blue line, the dephasing time is long and only the self-energy diagram is important. Hence, the factor $\mathcal{C}^{\phi}$ reduces to 1, and dephasing rate coincides with the out-scattering rate, τ_{out}^{-1}, obtained from the golden rule [8]. (In this calculation, q_c just provides an infrared cut-off.) Above the blue line, in regions I and II, both the self-energy and vertical diagrams are relevant, and the factor $\mathcal{C}^{\phi}(t)$ is important. Due to the extended structure of the correlation function of the FP pairs participating in the inelastic process, the influence of this factor on the dephasing rate is rather non-trivial, so that one cannot expand $\mathcal{C}^{\phi}(t)$.

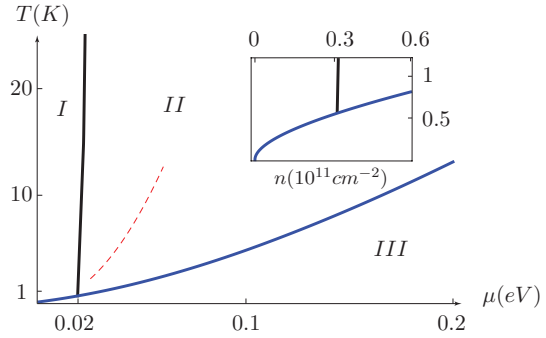

Figure 5.1: Phase diagram of the dephasing rate due to FPs with the scalar coupling. The blue and black lines divide the whole $(T-\mu)$ plane into three regions, see the text for explainations. The blue line coincides with the maximum of the dephasing rate as a function of chemical potential at a fixed temperature, see Fig. (5.2). The red dashed line representing a fragment of $\xi = 1$ is shown here for orientation. The inset is a zoom in of the intersection area of the blue and black lines plotted as a function of the electronic density.

In Fig. 5.1, the blue and black lines have been found by matching the asymptotic behavior of the dephasing rates deep in regions I, II and III. The blue line is defined by the criterion $\omega_{k_F}\tau_\phi \approx 3$, where τ_ϕ is calculated numerically from Eq. (4.1) with the phonon frequency ω_{k_F} taken from Eq. (2.2). The black line is obtained according to the equation $\omega_{q_c}\tau_\phi \approx 7$.

We introduce (μ_0, T_0) , the values of the crossing point of the blue and black lines as characteristic scales: $\mu_0 \sim \frac{\gamma}{c_\phi^2}\Delta_c$ and $T_0 \sim \frac{\gamma}{c_\phi^2}\mu_0$. Here, we have introduced $\gamma = \frac{\alpha\Delta_c}{v_F^2} \sim 0.02$, which is a parameter describing the adiabaticity of the el-FP interaction. Under a given choice of parameters, it can be found numerically that $\mu_0 \approx 0.02$eV and $T_0 \approx 0.6$K. The dephasing rate in different regions can be expressed as

$$\tau_\phi^{-1}(T) = \gamma T \times \begin{cases} 0.48\,(\mu/\mu_0)^{\frac{4-\eta}{8-5\eta}} & \text{I} \\ 0.18\sqrt{\mu/\mu_0} & \text{II} \\ 0.24\frac{T/T_0}{\mu/\mu_0}\log\xi^{-1} & \text{III.} \end{cases} \tag{5.1}$$

These expressions are obtained using asymptotic behavior of the function f in Eq. (4.1) and, therefore, are only applicable far away from the borderlines. (Note that all the coefficients are calculated based on the parameters we have chosen.) At low enough temperatures, $\mathcal{C}^\phi(t) = 1$ and the function $f(\mathcal{T}, \xi)$ is independent of $\mathcal{T}$. Hence, $\tau_\phi^{-1} \sim T^2$ in region III, which is a GR result. At high temperatures the phonons contributing to the electronic dephasing become quasi-static and, consequently, the dephasing rate is smaller than the out-scattering rate τ_{out}^{-1}. (For example, region II starts when $\tau_\phi^{-1}/\tau_{out}^{-1} \sim \frac{(\mu/\mu_0)^{3/2}}{T/T_0} < 1$.) Unlike region III, in regions I and II the dephasing rate is determined by a non-GR expression, and is proportional to temperature, irrespective of η. This is the main result of our paper.

Note that on the $(T-\mu)$ plane there exists another asymptotic region (IV), not mentioned in Eqs. (5.1). It lies at very small densities below the blue line and above the line $\xi = 1$. In this region, the dephasing rate is still described by the GR, but contrary to region III, renormalization of the FP spectrum at low momenta is essential. In this situation, the dephasing rate equals $\tau_\phi^{-1} \sim \gamma T\,(\mu/\mu_0)^{2\eta-1}\,(T/T_0)^{1-\eta}$. However, the relevant densities are so small, that this region does not fit into the scale of Fig. 5.1.

By comparing the rates in regions II and III, one may conclude that there should be a maximum in the dephasing rate as a function of μ. Indeed, as it is illustrated by Fig. 5.2 such a maximum exists. The line indicating the maximum essentially overlaps with the borderline between the regions I, II and the region III, which is illustrated by the blue line in Fig. 5.1.

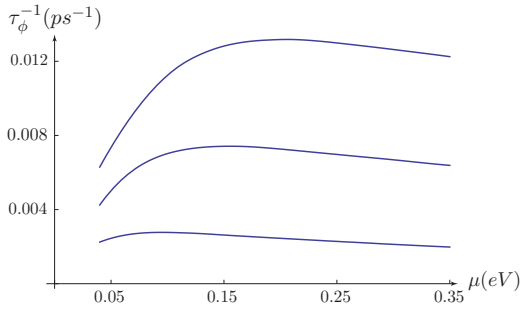

Figure 5.2: The dephasing rate as a function of the chemical potential. The lines are calculated at different temperatures, from top to buttom: T=15K, 10K, 5K.

The fluctuations of the vector potential are described by Eq. (2.6). Unlike the scalar potential, the dephasing rates induced by vector potential fluctuations are different for different channels owing to the factor $\mathcal{C}_l^A(\Omega,t) = 1 + s_l \frac{\sin \omega t}{\omega t}$, where $s_l = -1$ for the intervalley Cooperons ($l = 0, z$) and $s_l = 1$ for the intravalley Cooperons ($l = x, y$). In the static limit, the time reversal symmetry protects the intervalley channels from being dephased. On the contrary, for the intravalley channels, the static deformations produce dephasing. This happens because the electrons on the interfering trajectories are coupled to the vector potential of the same sign. The situation is similar to that for a particle in the random magnetic field [48, 49]. Unfortunately, the observation of this effect is obscured by the gaps inevitably produced in these channels by disorder scattering.

For the intervalley channels, the dephasing rate produced by the vector potential coupling is quite similar to its scalar counterpart, Eq. (5.1), with obvious modifications due to the change in the coupling constant and absence of screening for the vector potential. By contrast, for the intravalley channels (their rate is indicated by $*$), the rate changes from $2\tau_{*,A}^{-1}$ to $\tau_{*,A}^{-1}$ with increasing temperature, where

$$\tau_{*,A}^{-1} = \gamma T \begin{cases} 2.6\left(\mu/\mu_0'\right)^{2\eta-1}\left(T/T_0'\right)^{1-\eta} & \text{for } \xi \gg 1 \\ 1.9\sqrt{T/T_0'} & \text{for } \xi \ll 1 \end{cases} . \tag{5.2}$$

Here $\mu_0' = \left(c_\phi/c_A\right)^2 \mu_0$ and $T_0' = \left(c_\phi/c_A\right)^4 T_0$, where $c_A = \frac{g_2}{2\pi\rho\alpha^2} \sim 1.2$ is the dimensionless el-FPs coupling constant with vector potential fluctuations. Note that for $\xi \ll 1$, the characteristic momentum transfer is $\sim q_c$ instead of k_F. As a result, the rate is independent of the chemical potential.

6. DISCUSSION

Here we discuss some perculiar physics invovled in the problem. The turn to the linear behavior in T is related to the fact that at high temperatures phonons become slow on the timescale of τ_ϕ. It is instructive to compare this situation with the one for ordinary phonons in semiconductors , where the dephasing process can be viewed as coming from the energy diffusion via low-energy (i.e., quasi-elastic) collisions [44]. Under these conditions, the dephasing rate $\tau_\phi^{-1} \sim \sqrt{(\tau_\phi/\tau_{out})\,\delta\epsilon^2}$, where $\delta\epsilon$ denotes the characteristic energy transfer during a single scattering event. Thus, the accumulation of phase in the course of the energy diffusion yields $\tau_\phi^{-1} \sim \left(\delta\epsilon^2/\tau_{out}\right)^{1/3}$. The specific point of our problem, compared to dephasing via usual phonons, is that an electron is coupled to two flexural phonons, and dephasing cannot be described by the energy diffusion process. Because of this *two*-phonon interaction, the support of the correlation function of the fluctuations is not characterized by any typical frequency Ω, and frequency transfer occurs in such a way that typical energy transfer is of the order of $\tau_\phi^{-1}(T)$. In particular, this allows for an energy transfer exceeding T_{BG}, although the momentum transfer is limited by $2k_F$. As a result, the decay function $F_\phi(t)$ at short times (i.e., in the non-GR regime) is proportional to t^2, rather than t^3 as for the case of the energy diffusion. Note that the energy diffusion corresponds to the expansion of the factor $\mathcal{C}^\phi(t) \sim (\Omega t)^2$ which leads to the t^3-dependence of $F_\phi(t)$. As we have already mentioned, in the case of FPs one cannot expand $\mathcal{C}^\phi(t)$.

For completeness, let us discuss the dephasing due to the in-plane phonons [50] in graphene. For in-plane phonons, the Bloch-Grüneisen temperature $T_{BG}^{in} \approx 40\sqrt{n}$K. Below T_{BG}^{in}, the in-plane dephasing rate is $\sim T^4$ if the screening is taken into consideration, and $\sim T^2$ if the screening is irrelevant. For $T > T_{BG}^{in}$, the in-plane dephasing rate $\sim T$, and it is comparable with the dephasing rate due to the FPs [13, 51, 52]. For in-plane phonons, a region of non-GR dephasing rate, analogue to region II, develops at temperatures $\gtrsim \mu$ that is too high to be relevant.

The measured dephasing rate in graphene is usually compared to the contribution induced by the electron-electron interaction, τ_{ee}^{-1}, which is linear in T for $T < 1/\tau_{tr}$ [19]. However, the observed rate [20–22], when it is linear in T, always exceeds the theoretical estimation. Unlike other materials, in the case of graphene extrinsic sources for dephasing are limited. It is, therefore, important to analyze intrinsic mechanisms such as the interaction with the FPs. In view of the linear

dependence on T of the FP's contribution to dehpasing, it is reasonable to compare its value with τ_{ee}^{-1}. In principle, it is a competition between the two small parameters: the adiabatic parameter γ versus sheet resistance $\rho_{\square}$ measured in units of the quantum resistance. We compare the dephasing rates at density $n = 10^{12} cm^{-2}$ when the sheet resistance $\approx 0.5 k\Omega$. Under these conditions, both parameters γ and $\rho_{\square}$ are of the same value. Combining the contributions arising from the scalar and vector potentials, we obtain that $\tau_{FP}^{-1}/\tau_{ee}^{-1} \approx 0.2$. Next, the in-plane phonons generate a dephasing τ_{in}^{-1} that at $T < T_{BG}^{in}$ is negligible compared with τ_{FP}^{-1}, while at $T > T_{BG}^{in}$ they are comparable. It is important that each of the three rates: τ_{ee}^{-1}, τ_{FP}^{-1}, and τ_{in}^{-1}, has a distinct dependence on the chemical potential. While τ_{ee}^{-1} decreases with density, $\tau_{FP}^{-1} \propto \mu^{1/2}$ and $\tau_{in}^{-1} \propto \mu$. This opens a way to identify each of these mechanisms by studying the magnetoresistance as a function of the chemical potential. Furthermore, the sensitivity of the flexural phonons to a substrate can provide an additional possibility to identify τ_{FP}^{-1} in graphene through the electronic transport.

In our discussion, we always had in mind suspended graphene. However, our result may also be relevant even for supported samples when they are coupled to the substrate weakly enough by the Van der Waals forces [53]. One may expect that such a weak coupling does not provide an essential change in the phonon spectrum. Indeed, it is known that the phonon spectrum in graphene [54] and graphite [55] are practically identical for the corresponding branches. The Raman spectroscopy [56] also shows no change in the phonon spectrum due to the substrate. The FPs in the supported samples has been discussed recently in connection with the heat transport measurements in Refs. [9, 10].

Until now flexural phonons have been a delicate object to detect in electronic transport. We propose here to observe them through weak-localization measurements.

7. SUMMARY

We have analyzed a non-trivial contribution to the dephasing rate induced by the flexrual phonons in graphene. The softness of the spectrum, the smallness of the Bloch-Grüneisen tempeature for FPs and the simutanous coupling of two phonons with electrons all contribute to the non-trivial dephasing rate. We have evaluated the dephasing rate for a wide range of n and T, see Fig. 5.1 for the phase diagram. The dephasing rate τ_ϕ^{-1} can be separted into two parts in accord with the different coupling forms: scalar and vector potential coupling. In either coupling forms τ_ϕ^{-1} can be grouped into a scaling form, see Eq. (4.1) and Eq. (4.13). We also determined several asymptotic expressions for τ_ϕ^{-1}, see, for example, Eq. (5.1), which is our main result here. For scalar potential couplings, the calcuated τ_ϕ^{-1} shows a temperature dependence evolving from $\tau_\phi^{-1} \sim T^2$ to $\tau_\phi^{-1} \sim T$ when temperature increases. We also find τ_ϕ^{-1} to be a non-monotonous function of n. For vector potential couplings, the contribution should be further divided into two groups: intervalley and intravalley channels. The former one is similar to the scalar counterpart while the latter one has more peculiar density and temperature dependense, see Eq. (5.2). The estimated dephasing rate is smaller but still compartive to the contribution from the electron-electron interaction. These distinctive features of the new contribution can provide an effective way to identify flexural phonons in graphene through the electronic transport by measuring the weak localization corrections in magnetoresistance.

REFERENCES

[1] A. H. Castro Neto, N. M. R. Peres, K. S. Novoselov, and A. K. Geim, Reviews of Modern Physics **81**, 109 (2009).

[2] S. Das Sarma, S. Adam, E. H. Hwang, and E. Rossi, Reviews of Modern Physics **83**, 407 (2011).

[3] P. M. Chaikin and T. C. Lubensky, *Principles of condensed matter physics*, vol. 1 (Cambridge Univ Press, Cambridge, UK, 2000).

[4] D. R. Nelson and L. Peliti, Journal De Physique **48**, 1085 (1987).

[5] J. A. Aronovitz and T. C. Lubensky, Phys. Rev. Lett. **60**, 2634 (1988).

[6] E. Mariani and F. von Oppen, Phys. Rev. Lett. **100**, 076801 (2008).

[7] H. Ochoa, E. V. Castro, M. I. Katsnelson, and F. Guinea, Phys. Rev. B **83**, 235416 (2011).

[8] I. V. Gornyi, V. Y. Kachorovskii, and A. D. Mirlin, Phys. Rev. B **86**, 165413 (2012).

[9] A. A. Balandin, S. Ghosh, W. Bao, I. Calizo, D. Teweldebrhan, F. Miao, and C. N. Lau, Nano Letters **8**, 902 (2008).

[10] J. H. Seol et al., Science **328**, 213 (2010).

[11] K. I. Bolotin, K. J. Sikes, J. Hone, H. L. Stormer, and P. Kim, Phys. Rev. Lett. **101**, 096802 (2008).

[12] E. V. Castro, H. Ochoa, M. I. Katsnelson, R. V. Gorbachev, D. C. Elias, K. S. Novoselov, A. K. Geim, and F. Guinea, Phys. Rev. Lett. **105**, 266601 (2010).

[13] E. H. Hwang and S. Das Sarma, Phys. Rev. B **77**, 115449 (2008), note that the phonon's contribution to resistivity is about 100 Ohm on the background of few kOhms.

[14] E. Abrahams, P. W. Anderson, D. C. Licciardello, and T. V. Ramakrishnan, Phys. Rev. Lett. **42**, 673 (1979).

[15] P. A. Lee and T. V. Ramakrishnan, Reviews of Modern Physics **57**, 287 (1985).

[16] S. Chakravarty and A. Schmid, Physics Reports **140**, 193 (1986).

[17] F. V. Tikhonenko, D. W. Horsell, R. V. Gorbachev, and A. K. Savchenko, Phys. Rev. Lett. **100**, 056802 (2008).

[18] F. V. Tikhonenko, A. A. Kozikov, A. K. Savchenko, and R. V. Gorbachev, Phys. Rev. Lett. **103** (2009).

[19] B. L. Altshuler, A. G. Aronov, and D. E. Khmelnitsky, Journal of Physics C-Solid State Physics **15**, 7367 (1982).

[20] X. Wu, X. Li, Z. Song, C. Berger, and W. A. de Heer, Phys. Rev. Lett. **98**, 136801 (2007).

[21] F. V. Tikhonenko, A. A. Kozikov, A. K. Savchenko, and R. V. Gorbachev, Phys. Rev. Lett. **103**, 226801 (2009).

[22] M. B. Lundeberg and J. A. Folk, Phys. Rev. Lett. **105**, 146804 (2010).

[23] H. Suzuura and T. Ando, Phys. Rev. B **65**, 235412 (2002).

[24] M. A. H. Vozmediano, M. I. Katsnelson, and F. Guinea, Physics Reports-Review Section of Physics Letters **496**, 109 (2010).

[25] F. Guinea, Solid State Communications **152**, 1437 (2012).

[26] N. Levy, S. A. Burke, K. L. Meaker, M. Panlasigui, A. Zettl, F. Guinea, A. H. Castro Neto, and M. F. Crommie, Science **329**, 544 (2010).

[27] F. Guinea, M. I. Katsnelson, and A. K. Geim, Nature Physics (2009).

[28] F. de Juan, A. Cortijo, M. A. H. Vozmediano, and A. Cano, Nature Physics **7**, 810 (2011).

[29] T. Low and F. Guinea, Nano Lett **10**, 3551 (2010).

[30] A. Fasolino, J. H. Los, and M. I. Katsnelson, Nature Materials **6**, 858 (2007).

[31] P. A. Lee, Phys. Rev. Lett. **63**, 680 (1989).

[32] N. Nagaosa and P. A. Lee, Phys. Rev. Lett. **64**, 2450 (1990).

[33] D. K. Efetov and P. Kim, Phys. Rev. Lett. **105**, 256805 (2010).

[34] J. C. W. Song, M. Y. Reizer, and L. S. Levitov, Phys. Rev. Lett. **109**, 106602 (2012).

[35] J. von Delft, F. Marquardt, R. A. Smith, and V. Ambegaokar, Phys. Rev. B **76**, 195332 (2007).

[36] A. P. Levanyuk, Soviet Physics JETP **9**, 571 (1959).

[37] V. L. Ginzburg, Soviet Physics-Solid State **2**, 1824 (1961).

[38] D. Nelson, T. Piran, and S. Weinberg, *Statistical Mechanics of Membranes and Surfaces* (World Scientific Pub., Singapore, 2004).

[39] P. Le Doussal and L. Radzihovsky, Phys. Rev. Lett. **69**, 1209 (1992).

[40] K. V. Zakharchenko, R. Roldan, A. Fasolino, and M. I. Katsnelson, Phys. Rev. B **82**, 125435 (2010).

[41] V. N. Kotov, B. Uchoa, V. M. Pereira, F. Guinea, and A. H. Castro Neto, Reviews of Modern Physics **84**, 1067 (2012).

[42] D. Gazit, Phys. Rev. E **80** (2009).

[43] B. L. Altshuler, D. Khmelnitzkii, A. I. Larkin, and P. A. Lee, Phys. Rev. B **22**, 5142 (1980).

[44] B. L. Altshuler, A. G. Aronov, and D. E. Khmelnitsky, Solid State Communications **39**, 619 (1981).

[45] E. McCann, K. Kechedzhi, V. I. Fal'ko, H. Suzuura, T. Ando, and B. L. Altshuler, Phys. Rev. Lett. **97**, 146805 (2006).

[46] W. Eiler, Journal of Low Temperature Physics **56**, 481 (1984).

[47] F. Marquardt, J. von Delft, R. A. Smith, and V. Ambegaokar, Phys. Rev. B **76**, 195331 (2007).

[48] A. Aronov, A. Mirlin, and P. Wölfle, Physical Review B **49**, 16609 (1994).

[49] A. G. Aronov and P. Wölfle, Phys. Rev. B **50**, 16574 (1994).

[50] J. Rammer and A. Schmid, Phys. Rev. B **34**, 1352 (1986).

[51] E. Mariani and F. von Oppen, Phys. Rev. B **82**, 195403 (2010).

[52] Q. Li and S. Das Sarma, Phys. Rev. B **87**, 085406 (2013).

[53] A. K. Geim and I. V. Grigorieva, Nature **499**, 419 (2013).

[54] D. L. Nika, E. P. Pokatilov, A. S. Askerov, and A. A. Balandin, Phys. Rev. B **79**, 155413 (2009).

[55] R. Al-Jishi and G. Dresselhaus, Phys. Rev. B **26**, 4514 (1982).

[56] Y. Y. Wang et al., The Journal of Physical Chemistry C **112**, 10637 (2008).